

# Three-dimensional imaging using continuously self-imaging gratings

Martin Piponnier,<sup>1,\*</sup> Guillaume Druart,<sup>2</sup> Ryoichi Horisaki,<sup>3</sup> Nicolas Guérineau,<sup>2</sup>

Jérôme Primot,<sup>2</sup> Laurent Mugnier,<sup>2</sup> and François Goudail<sup>1</sup>

<sup>1</sup>Laboratoire Charles Fabry, UMR 8501, Institut d'Optique, CNRS, Univ Paris Sud 11, 2, Avenue Augustin Fresnel, 91127 Palaiseau, France

<sup>2</sup>ONERA—The French Aerospace Laboratory, Palaiseau F-91761, France

<sup>3</sup>Department of Information and Physical Sciences, Graduate School of Information Science and Technology, Osaka University, 1-5 Yamadaoka, Suita, Osaka 565-0871, Japan

\*Corresponding author: martin.piponnier@institutoptique.fr

Received July 11, 2013; revised August 29, 2013; accepted August 31, 2013;  
posted September 9, 2013 (Doc. ID 193769); published October 7, 2013

In this Letter, we propose a method to perform 3D imaging with a simple and robust imaging system only composed of a continuously self-imaging grating (CSIG) and a matrix detector. With a CSIG, the intensity pattern generated by an object source is periodic and propagation invariant, apart from a dilatation factor that depends on the distance of the object. We demonstrate, theoretically and experimentally, how to exploit this property to analyze a scene in three dimensions. Such an imaging system can be used, for example, for tomographic applications.

*OCIS codes:* (050.1950) Diffraction gratings; (070.2025) Discrete optical signal processing; (070.3185) Invariant optical fields; (110.2970) Image detection systems; (110.6880) Three-dimensional image acquisition.

<http://dx.doi.org/10.1364/OL.38.004058>

We observe that many efforts are currently done to develop imaging systems that deliver not only an image from the observed scene, but also additional information such as depth [1], spectrum [2], or polarization state [3,4], for example. This approach has been particularly successful in the domain of 3D imaging. In this domain, different optical designs have been proposed that provide an image of the observed scene and a distance measurement of the objects present in the scene [1]. The distance information can be obtained through different imaging properties such as stereoscopic vision [5] or a dependency of the point-spread function to the object distance thanks to aperture coding [6,7]. Many optical designs based on these properties were proposed for numerous applications in medicine [8], security [9], or metrology [10].

Analysis of the different 3D imaging systems shows that the distance information is generally obtained at the expense of another performance: resolution in stereoscopic multichannel imaging systems [5], image quality in imaging systems based on depth from defocus [1], or integration time in scanning imaging systems.

In this Letter, we propose a method to perform 3D imaging with a system composed of a continuously self-imaging grating (CSIG) [11] and a matrix detector placed at a distance  $F$  of the grating. We will demonstrate that this system performs 3D imaging with a simple and robust architecture and by grabbing only a single image. Furthermore, we will show how the distance information is obtained at the expense of the amount of information contained in the image of the observed scene.

The CSIG is a diffractive optical element that diffracts a finite number  $N$  of orders. The transmittance function of the CSIG, denoted by  $t$ , is chosen so that these diffracted orders generate an intensity pattern that is propagation invariant along the  $z$  axis. Montgomery [12] and Durnin [13] defined the condition to get a propagation-invariant beam: the Fourier transform (FT) of the

transmittance must be located on a ring, called the Montgomery ring. Guérineau *et al.* adapted this condition to the case of gratings [11]. The CSIG is defined by the FT of its transmittance, denoted by  $T$ , which is the intersection between a Montgomery ring of radius  $\rho_0$  and a Cartesian grid of pitch  $1/a_0$ . It can be described in the Fourier domain as a set of  $N$  Dirac peaks of relative weight  $c_k$  and whose coordinates on the Cartesian grid are given by the couple of integers  $(p_k, q_k)$ . The general expression for  $T$  is thus the following:

$$T(f_x, f_y) = \sum_{k=1}^N c_k \delta\left(f_x - \frac{p_k}{a_0}, f_y - \frac{q_k}{a_0}\right), \quad (1)$$

where  $\delta$  is the Dirac distribution, and the coordinates  $(p_k, q_k)$  satisfy the circle's equation:

$$\frac{p_k^2}{a_0^2} + \frac{q_k^2}{a_0^2} = \rho_0^2 = \frac{\eta^2}{a_0^2}, \quad (2)$$

where  $\eta^2$  is an integer that characterizes the CSIG. A consequence of this definition is that the transmittance  $t$ , deduced from  $T$  by inverse FT, is 2D periodic in the transverse plane  $(x, y)$  of period  $a_0$ .

If the device is illuminated by a point source located at infinity on the  $z$  axis and of intensity  $I_0$ , it has been demonstrated [11,13] that the propagated intensity pattern, called  $I_{\text{ref}}$ , does not depend on  $z$  and is given by

$$I_{\text{ref}}(x, y) = I_0 |t(x, y)|^2. \quad (3)$$

$I_{\text{ref}}$  represents the reference image observed on the detector for a point source located at infinity. Like the transmittance,  $I_{\text{ref}}$  is also 2D periodic of period  $a_0$  in the transverse plane. From Eq. (3), we can deduce that the spatial frequency spectrum of the reference image, called  $\tilde{I}_{\text{ref}}$ , is linked to the autocorrelation of  $T$ :

$$\tilde{I}_{\text{ref}}(f_x, f_y) = I_0[T \otimes T](f_x, f_y), \quad (4)$$

where  $\otimes$  is the correlation product. From Eqs. (1) and (4), we can deduce that the reference spectrum is composed of a finite number  $N' = N^2/2 + 1$  of Dirac peaks located on the Cartesian grid of pitch  $1/a_0$  and on a disk of radius  $f_c = 2\eta/a_0$ , which is the cutoff frequency of the CSIG. The first important property for 3D imaging is that this reference spectrum, which we will identify to the optical transfer function (OTF) of the CSIG, is discrete in the Fourier domain. Figure 1 illustrates the functions  $T$ ,  $I_{\text{ref}}$ , and  $\tilde{I}_{\text{ref}}$  for a CSIG of parameter  $\eta^2 = 325$ .

Let us now consider that the device is illuminated by a point source of the same intensity but located at a finite distance  $d$  of the CSIG. In the approximation of geometrical optics, the intensity pattern, denoted by  $I$ , can be described by the following expression [14]:

$$I(x, y) = \frac{1}{\Delta^2} I_{\text{ref}}\left(\frac{x}{\Delta}, \frac{y}{\Delta}\right), \quad (5)$$

where  $\Delta$  is a dilatation factor given by

$$\Delta = 1 + \frac{F}{d}, \quad (6)$$

where  $F$  is the distance between the CSIG and the detector. The image  $I$  obtained on the detector is thus dilated compared to the reference image  $I_{\text{ref}}$ . From Eq. (5), we can deduce that the spatial frequency spectrum of the image, denoted by  $\tilde{I}$ , is contracted by a factor of  $C$  compared to the reference spectrum  $\tilde{I}_{\text{ref}}$ :

$$\tilde{I}(f_x, f_y) = C \tilde{I}_{\text{ref}}\left(\frac{f_x}{C}, \frac{f_y}{C}\right), \quad (7)$$

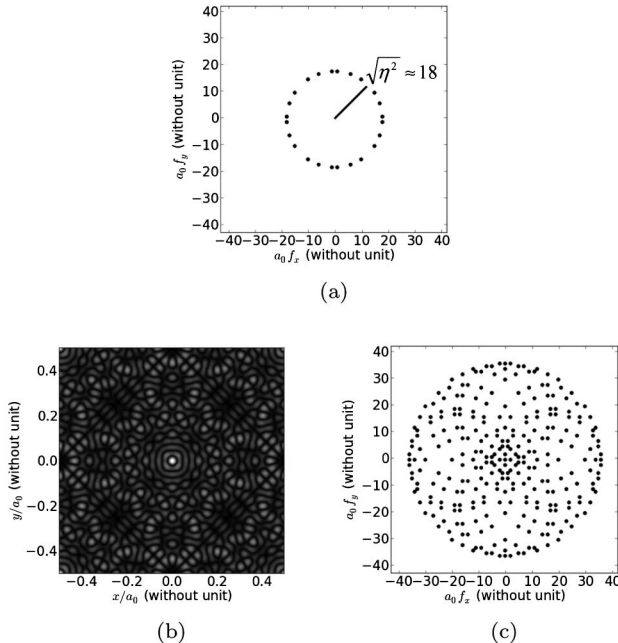


Fig. 1. Illustration of (a)  $T$ , (b)  $I_{\text{ref}}$ , and (c)  $\tilde{I}_{\text{ref}}$  for a CSIG of parameter  $\eta^2 = 325$  that diffracts  $N = 24$  orders. For  $I_{\text{ref}}$ , only an elementary pattern of size  $a_0 \times a_0$  is represented.

where  $C$  is the contraction factor defined by

$$C = \frac{1}{\Delta} = \frac{d}{d + F}. \quad (8)$$

Thus, thanks to the propagation-invariance property of a CSIG, only the coordinates of the  $N'$  Dirac peaks that compose  $I$  depend on the object distance  $d$  and not their complex amplitudes. We will use these two properties (lacunarity and contraction in Fourier domain) to perform 3D imaging.

If the observed scene is composed of a set of  $n$  incoherent point sources of different intensities  $I_i$  and located at different distances  $d_i$  from the CSIG, the image seen by the detector is the sum of the intensity patterns generated by each point source:

$$I(x, y) = \sum_{i=1}^n \frac{I_i}{\Delta_i^2} I_0 \left( \frac{x}{\Delta_i}, \frac{y}{\Delta_i} \right). \quad (9)$$

Since FT is a linear operation, the spectrum of the recorded intensity pattern is the sum of the spectra generated by each source:

$$\tilde{I}(f_x, f_y) = \sum_{i=1}^n I_i C_i \frac{\tilde{I}_{\text{ref}}}{I_0} \left( \frac{f_x}{C_i}, \frac{f_y}{C_i} \right). \quad (10)$$

As the spectrum generated by a point source through a CSIG is lacunar and is contracted depending on the distance  $d$  of the object, it is possible to distinguish in the Fourier domain the signals generated by each point source. Figure 2 illustrates this signal separation in the Fourier domain for two point sources located at the distances  $d_1 = \infty$  and  $d_2 = 710$  mm from the CSIG.

The CSIG can thus be seen as a device that cuts the object space into numerous layers at different distances from it, transmits a finite number  $N'$  of spatial frequencies that compose the intensity pattern in this layer, multiplexes all information on a single image on the detector, and all information can be separated by simply performing an FT operation. However, the lacunarity of the OTF leads to the sampling of the spatial frequency spectrum of an object located in a layer. In our case, the 3D information is thus obtained at the expense of the amount of

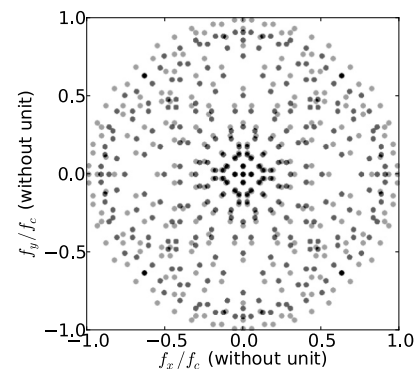


Fig. 2. Illustration of separated spectra generated by two point sources at the distances  $d_1 = \infty$  (light gray dots) and  $d_2 = 710$  mm (dark gray dots) from the CSIG.

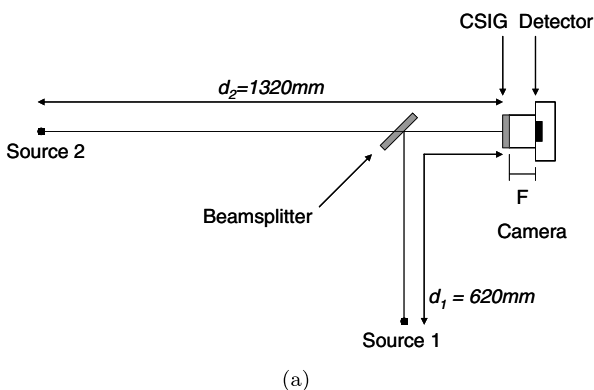
information on the observed objects, and image processing is necessary to reconstruct a reliable image of the scene [15,16].

To demonstrate the 3D capability of this system, we made a CSIG of parameters  $a_0 = 7.5$  mm and  $\eta^2 = 9425$  and of diameter  $D = 50$  mm. This CSIG diffracts  $N = 48$  orders and  $\tilde{I}_{\text{ref}}$  is composed of  $N' = 1153$  Dirac peaks. The CSIG was mounted on a visible DALSA camera, which has a  $1024 \times 1024$  matrix detector of pitch  $p = 12$   $\mu\text{m}$ . The distance between the CSIG and the detector was set to  $F = 61.7$  mm. The scene was composed of two point sources at distances  $d_1 = 620$  mm and  $d_2 = 1320$  mm. A scheme of this setup is given in Fig. 3(a). We obtained the experimental image illustrated in Fig. 3(b).

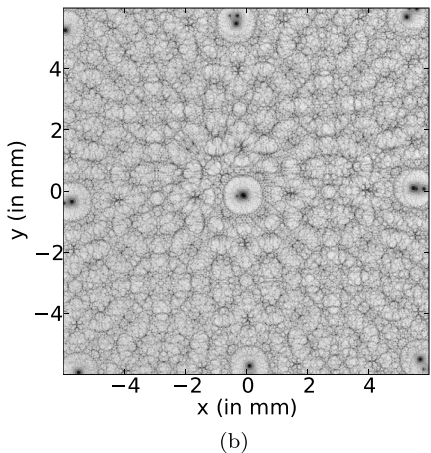
To distinguish the signals from each source, we perform a scan in the Fourier domain. It means we compute the product between the measured spectrum  $\tilde{I}$  and the reference spectrum  $\tilde{I}_{\text{ref}}$  contracted by a factor of  $C$ . We get a *correlation* curve, denoted by  $\text{cor}(C)$ , which is expressed by

$$\text{cor}(C) = \iint_{\mathbb{R}^2} \tilde{I}(f_x, f_y) \times \tilde{I}_{\text{ref}}\left(\frac{f_x}{C}, \frac{f_y}{C}\right) df_x df_y. \quad (11)$$

We calculate this correlation curve for a contraction factor  $C$  in the range  $[0.5, 1]$ , which corresponds to a scan of



(a)



(b)

Fig. 3. (a) Scheme of the setup used to image two point sources at different distances from the CSIG. (b) Experimental image (in reversed contrast) obtained with this setup.

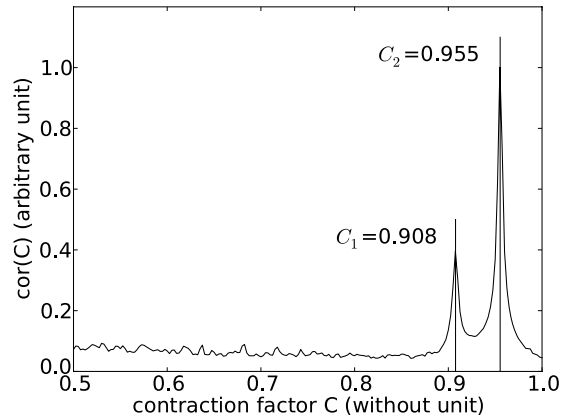


Fig. 4. Illustration of the correlation between the experimental spectrum and the reference spectrum contracted by a factor of  $C$  varying in the range  $[0.5, 1]$ .

the object space from an arbitrary closest distance  $d = F$  to infinity. Figure 4 illustrates the correlation curve obtained with the experimental setup.

On this figure, we clearly distinguish two peaks indicating the presence of light sources at two different distances. For the first peak, the contraction factor is equal to  $C_1 = 0.908$ , which corresponds to a distance of  $d_1 = 607$  mm by using Eqs. (6) and (8). For the second peak, the contraction factor is equal to  $C_2 = 0.955$ , which corresponds to a distance of  $d_2 = 1319$  mm. These measured distances are close to the real ones, so we demonstrate this way the ability of CSIG to estimate distance information.

To demonstrate the 3D imaging capability, we replaced the point sources by two spatially extended objects: a triangle of size 13 mm and a square of size 10 mm. The setup and the obtained experimental image are illustrated in Fig. 5. As noted, we performed the scan in the Fourier domain, and we obtained a *correlation* curve with two peaks, where the first one at  $C_1 = 0.889$  corresponds to a distance  $d_1 = 493$  mm, and the second one at  $C_2 = 0.942$  corresponds to a distance  $d_2 = 1004$  mm.

Thanks to this operation, we know that some luminous objects are present in two different layers of the object space. To get more information about these objects, we measured the complex amplitude of the spectrum at the  $N'$  spatial frequencies that compose the OTF, for the contraction factors  $C_1$  and  $C_2$ . For each contraction factor, this set of complex values is a sampling of the spatial frequency spectrum of the observed object. We performed an inverse FT on both sets of values to get two separated images, one per object. Then, to restore each image, we used the prior knowledge that the object is flat and not textured. In this case, we can apply a particular compressed sensing algorithm described in [16] and use the sparsity of the object in the total variation domain to reconstruct it. We applied this reconstruction method on the images obtained with  $C_1 = 0.889$  then with  $C_2 = 0.942$ , and we obtained the reconstructed images given, respectively, in Figs. 6(a) and 6(b).

On the reconstructed images of Fig. 6, we clearly recognize the triangle located at a distance  $d_1 = 485$  mm and the square located at a distance  $d_2 = 995$  mm. The size of images is reduced compared to the size of objects

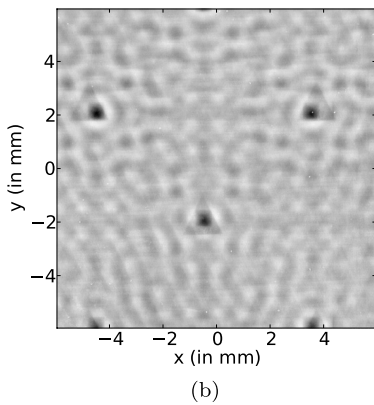
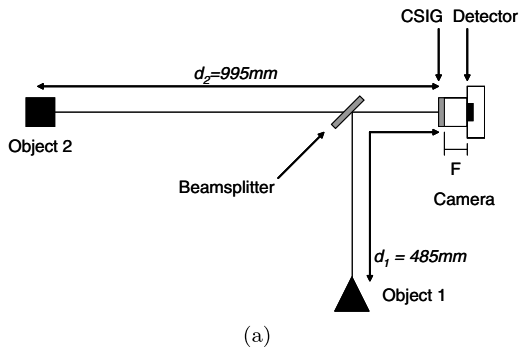


Fig. 5. (a) Scheme of the setup used to image two extended objects at different distances of the CSIG. (b) Experimental image (in reversed contrast) obtained with this setup.

because of the magnification ratio  $M = F/d$  introduced by the setup [16]. Moreover, the objects are well reconstructed here because the size of each object was chosen inside the validity domain of this reconstruction method, which was already discussed in [16]. We demonstrate this way that it is possible to measure the distance of the objects present in the observed scene and also to get a correct image of these objects, thanks to an appropriate image-processing method.

In conclusion, we demonstrated in this Letter that a simple and robust imaging system, only composed of a CSIG and a matrix detector, can be used for 3D imaging. With this optical design, the object distance is obtained at the expense of the amount of information in the transverse image, but we demonstrated experimentally that it is possible to reconstruct the objects with image processing. This device can thus be used for tomographic

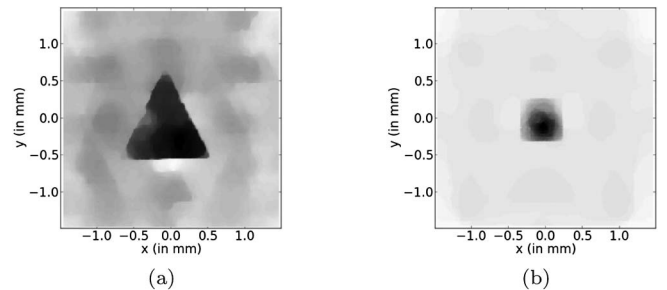


Fig. 6. Illustration of the reconstructed objects (in reversed contrast) located at a distance (a)  $d_1 = 493$  mm and (b)  $d_2 = 1004$  mm.

applications in simple scenes. Further work is in progress to estimate the influence of noise on the 3D estimation precision and to develop image-processing methods adapted to 3D imaging with a CSIG.

## References

1. C. Zhou, S. Lin, and S. Nayar, IEEE **978**, 325 (2009).
  2. N. Guérineau, G. Druart, F. Gillard, Y. Ferrec, M. Chambon, S. Rommeluère, G. Vincent, R. Haïdar, J. Taboury, and M. Fendler, Proc. SPIE **8012**, 801229 (2011).
  3. B. Laude-Boulesteix, A. De Martino, B. Drevillon, and L. Schwartz, Appl. Opt. **43**, 2824 (2004).
  4. G. Anna, H. Sauer, F. Goudail, and D. Dolfi, Appl. Opt. **51**, 5302 (2012).
  5. R. Horisaki, S. Irie, Y. Ogura, and J. Tanida, Opt. Rev. **14**, 347 (2007).
  6. Y. Bando, B.-Y. Chen, and T. Nishita, ACM Trans. Graph. **27**, 134 (2008).
  7. S. McEldowney, "Use of wavefront coding to create a depth image," U.S. patent application 20110310226 (December 22, 2011).
  8. M. Levoy, R. Ng, A. Adams, M. Footer, and M. Horowitz, ACM Trans. Graph. **25**, 924 (2006).
  9. A. Koschan, M. Pollefeys, and M. Abidi, *3D Imaging for Safety and Security*, Computational Imaging and Vision (Springer, 2007), Vol. **35**.
  10. P. J. Besl, Mach. Vis. Appl. **1**, 127 (1988).
  11. N. Guérineau, B. Harchaoui, J. Primot, and K. Heggarty, Opt. Lett. **26**, 411 (2001).
  12. W. D. Montgomery, J. Opt. Soc. Am. **57**, 772 (1967).
  13. J. Durnin, J. Opt. Soc. Am. A **4**, 651 (1987).
  14. D. Joyeux and Y. Cohen-Sabban, Appl. Opt. **21**, 625 (1982).
  15. M. Piponnier, R. Horisaki, G. Druart, N. Guérineau, A. Kattning, and J. Primot, Opt. Lett. **37**, 3492 (2012).
  16. R. Horisaki, M. Piponnier, G. Druart, N. Guérineau, J. Primot, F. Goudail, J. Taboury, and J. Tanida, Appl. Opt. **52**, 3802 (2013).